

ACCEPTED MANUSCRIPT • OPEN ACCESS

## Soil respiration strongly offsets carbon uptake in Alaska and Northwest Canada

To cite this article before publication: Jennifer Watts *et al* 2021 *Environ. Res. Lett.* in press <https://doi.org/10.1088/1748-9326/ac1222>

### Manuscript version: Accepted Manuscript

Accepted Manuscript is “the version of the article accepted for publication including all changes made as a result of the peer review process, and which may also include the addition to the article by IOP Publishing of a header, an article ID, a cover sheet and/or an ‘Accepted Manuscript’ watermark, but excluding any other editing, typesetting or other changes made by IOP Publishing and/or its licensors”

This Accepted Manuscript is © 2021 The Author(s). Published by IOP Publishing Ltd.

As the Version of Record of this article is going to be / has been published on a gold open access basis under a CC BY 3.0 licence, this Accepted Manuscript is available for reuse under a CC BY 3.0 licence immediately.

Everyone is permitted to use all or part of the original content in this article, provided that they adhere to all the terms of the licence <https://creativecommons.org/licenses/by/3.0>

Although reasonable endeavours have been taken to obtain all necessary permissions from third parties to include their copyrighted content within this article, their full citation and copyright line may not be present in this Accepted Manuscript version. Before using any content from this article, please refer to the Version of Record on IOPscience once published for full citation and copyright details, as permissions may be required. All third party content is fully copyright protected and is not published on a gold open access basis under a CC BY licence, unless that is specifically stated in the figure caption in the Version of Record.

View the [article online](#) for updates and enhancements.

**Title: Soil Respiration Strongly Offsets Carbon Uptake in Alaska and Northwest Canada**

Jennifer D. Watts<sup>1</sup>, Susan M. Natali<sup>1</sup>, Christina Minions<sup>2</sup>, Dave Risk<sup>3</sup>, Kyle Arndt<sup>4</sup>, Donatella Zona<sup>5</sup>, Eugénie S. Euskirchen<sup>6</sup>, Adrian V. Rocha<sup>7</sup>, Oliver Sonnentag<sup>8</sup>, Manuel Helbig<sup>9</sup>, Aram Kalhori<sup>10</sup>, Walt Oechel<sup>5</sup>, Hiroki Ikawa<sup>11</sup>, Masahito Ueyama<sup>12</sup>, Rikie Suzuki<sup>13</sup>, Hideki Kobayashi<sup>13</sup>, Gerardo Celis<sup>14,15</sup>, Edward A G Schuur<sup>15</sup>, Elyn Humphreys<sup>16</sup>, Yongwon Kim<sup>17</sup>, Bang-Yong Lee<sup>18</sup>, Scott Goetz<sup>15</sup>, Nima Madani<sup>19</sup>, Luke D. Schiferl<sup>20</sup>, Roisin Commane<sup>20</sup>, John S Kimball<sup>21</sup>, Zhihua Liu<sup>21</sup>, Margaret S Torn<sup>22</sup>, Stefano Potter<sup>1</sup>, Jonathan A. Wang<sup>23</sup>, M. Torre Jorgenson<sup>24</sup>, Jingfeng Xiao<sup>25</sup>, Xing Li<sup>25</sup>, Colin Edgar<sup>6</sup>

<sup>1</sup>Woodwell Climate Research Center, 149 Woods Hole Rd, Falmouth, MA 02540-1644, USA

<sup>2</sup>University of Alaska, Anchorage, 3211 Providence Dr, Anchorage, AK 99508, USA

<sup>3</sup>St. Francis Xavier University, 4130 University Ave, Antigonish, Nova Scotia, CA

<sup>4</sup>University of New Hampshire, 105 Main St, Durham, NH, 03824, USA

<sup>5</sup>San Diego State University, 5500 Campanile Dr, San Diego, CA, 92182, USA

<sup>6</sup>University of Alaska, Fairbanks, Institute of Arctic Biology, 2140 Koyukuk Dr. P.O. Box 757000, Fairbanks, AK, 99775, USA

<sup>7</sup>University of Notre Dame, 100 Galvin Life Science Center, Notre Dame, IN, 46556, USA

<sup>8</sup>University of Montreal, P.O. Box 6128 Centre-Ville STN Montreal, QC, H3C 3J7, CA

<sup>9</sup>Dalhousie University, 6310 Coburg Rd, Halifax, NS, B3H 4R2, CA

<sup>10</sup>GFZ German Research Centre for Geoscience, Helmholtz Center, Telegrafenberg 14473 Potsdam, DE

<sup>11</sup>Institute for Agro-Environmental Sciences, NARO, 3-1-3 Kannondai, Tsukuba, Ibaraki, JP

<sup>12</sup>Osaka Prefecture University, 1-1 Gakuen-cho, Naka-ku, Sakai, JP

<sup>13</sup>JAMSTEC-Japan Agency for Marine-Earth Science and Technology, 3172-25, Showa-machi, Kanazawa-ku, Yokohama, Kanagawa, JP

<sup>14</sup>University of Florida, Gainesville, FL, 32611, USA

<sup>15</sup>Northern Arizona University, P.O. Box 5620, Flagstaff, AZ, 86011, USA

<sup>16</sup>Carleton University, 1125 Colonel By Dr, Ottawa, ON, K1S 5B6, CA

<sup>17</sup>International Arctic Research Center (IARC), University of Alaska Fairbanks, AK 99775, USA

<sup>18</sup>Korea Polar Research Institute, 26 Songdomirae-ro, Yeonsu-go, Incheon, KR

<sup>19</sup>Jet Propulsion Laboratory, 4800 Oak Grove Dr, Pasadena, CA, 91109, USA

<sup>20</sup>Lamont-Doherty Earth Observatory, Columbia University, Palisades, NY 10964, USA

<sup>21</sup>NTSG, University of Montana, ISB 415, 32 Campus Drive, Missoula, MT 59812, USA

<sup>22</sup>Lawrence Berkeley National Lab, 084 M/S 74R316C, 1 Cyclotron Rd, Berkeley, CA, 94720, USA

<sup>23</sup>University of California Irvine, Croul Hall, Irvine, CA, 92697-3100.

<sup>24</sup>Alaska Ecosystem Science, 2332 Cordes Way, Fairbanks, AK, 99709, USA

<sup>25</sup>Earth Systems Research Center, Institute for the Study of Earth, Oceans, and Space, University of New Hampshire, Durham NH 03824, USA

**Abstract**

Soil respiration (i.e., from soils and roots) provides one of the largest global fluxes of carbon dioxide ( $\text{CO}_2$ ) to the atmosphere and is likely to increase with warming, yet the magnitude of soil respiration from rapidly thawing Arctic-boreal regions is not well understood. To address this knowledge gap, we first compiled a new  $\text{CO}_2$  flux database for permafrost-affected tundra and boreal ecosystems in Alaska and Northwest Canada. We then used the  $\text{CO}_2$  database, multi-sensor satellite imagery, and Random Forest models to assess the regional magnitude of soil respiration. The flux database includes a new Soil Respiration Station network of chamber-based fluxes, and fluxes from eddy covariance towers. Our site-level data, spanning September 2016 to August 2017, revealed that the largest soil respiration emissions occurred during the summer (June-August) and that summer fluxes were higher in boreal sites ( $1.87 \pm 0.67 \text{ gCO}_2\text{-C m}^{-2} \text{ d}^{-1}$ ) relative to tundra ( $0.94 \pm 0.4 \text{ gCO}_2\text{-C m}^{-2} \text{ d}^{-1}$ ). We also observed considerable emissions (boreal:  $0.24 \pm 0.2 \text{ gCO}_2\text{-C m}^{-2} \text{ d}^{-1}$ ; tundra:  $0.18 \pm 0.16 \text{ gCO}_2\text{-C m}^{-2} \text{ d}^{-1}$ ) from soils during the winter (November-March) despite frozen surface conditions. Our model estimates indicated an annual region-wide loss from soil respiration of  $591 \pm 120 \text{ Tg CO}_2\text{-C}$  during the 2016-2017 period. Summer months contributed to 58% of the regional soil respiration, winter months contributed to 15%, and the shoulder months contributed to 27%. In total, soil respiration offset 54% of annual gross primary productivity (GPP) across the study domain. We also found that in tundra environments, transitional tundra/boreal ecotones, and in landscapes recently affected by fire, soil respiration often exceeded GPP, resulting in a net annual source of  $\text{CO}_2$  to the atmosphere. As this region continues to warm, soil respiration may increasingly offset GPP, further amplifying global climate change.

**Keywords:** Arctic, boreal, soil respiration, roots, carbon,  $\text{CO}_2$ , winter, ecosystem vulnerability, climate change

## 1 2 3 74 **1. Introduction**

4  
5 75 The northern permafrost region holds over 50% of the global soil organic carbon (SOC) pool and  
6 approximately one trillion tonnes of carbon in the top 3-m of soil alone (Hugelius *et al* 2014,  
7 Meredith *et al* 2019). Historically, SOC in permafrost-affected ground and seasonally thawed  
8 active layers was largely protected from microbial decomposition by low-temperatures  
9 (Faucherre *et al* 2018). However, arctic air temperatures have increased rapidly (Box *et al* 2019),  
10 rising 2.7 °C (annual average) and 3.1 °C (October – May) between 1971 to 2017. This warming  
11 has increased the length of the non-frozen season (Kim *et al* 2012) and has deepened soil thaw  
12 (Luo *et al* 2016) in Alaska and Canada. Soil warming can increase microbial activity (Natali *et al*  
13 2014) and may result in large amounts of soil carbon being released into the atmosphere,  
14 predominantly as carbon dioxide (CO<sub>2</sub>; Schuur *et al* 2015, Turetsky *et al* 2020).

15  
16 85 Soil root and microbial respiration (herein referred to as soil respiration) are dominant  
17 components of an ecosystem's annual CO<sub>2</sub> emission (Mahecha *et al* 2010). Soil respiration in  
18 boreal forests is estimated to account for 48–68% of total ecosystem respiration (ER; soil +  
19 aboveground components; Hermle *et al* 2010, Parker *et al* 2020). In tundra, soil respiration is the  
20 primary source of CO<sub>2</sub> efflux and summer emissions alone may account for 60–90% of annual  
21 ER (Sommerkorn *et al* 1999, Gagnon *et al* 2018, Strimbeck *et al* 2018). Generally, the  
22 seasonality and magnitude of soil respiration are influenced by soil temperature, soil water  
23 content, root activity, and microbial-community access to SOC (Bond-Lamberty *et al* 2004,  
24 Schuur *et al* 2009, Nagano *et al* 2018).

25  
26 94 As northern landscapes continue to warm, CO<sub>2</sub> emissions resulting from soil respiration may  
27 increasingly offset carbon uptake by plants (i.e., gross primary productivity, GPP). Moreover, the  
28 fastest rate of warming in the Arctic-boreal region is occurring in autumn, winter, and spring  
29 (Box *et al* 2019), a period when microbial respiration continues but plant productivity is limited.  
30 Recent tundra and boreal carbon budgets in northern Alaska and Canada using eddy covariance  
31 (EC) flux observations show that enhanced soil respiration during an anomalously warm winter  
32 (2015-2016) offset any carbon gains provided by GPP (Liu *et al* 2020). Similarly, annual soil  
33 respiration offset 75% of the total forest GPP in a boreal Finland study (Pumpanen *et al* 2015). In  
34 northern Sweden, a steady increase in soil respiration, and no change in forest GPP, resulted in a  
35 transition from net annual ecosystem CO<sub>2</sub> sink to source (Hadden *et al* 2016). An atmospheric  
36 study of North Slope, Alaska tundra reported late autumn and early winter CO<sub>2</sub> emissions had  
37  
38  
39  
40  
41  
42  
43  
44  
45  
46  
47  
48  
49  
50  
51  
52  
53  
54  
55  
56  
57  
58  
59  
60

1  
2  
3 105 increased by 73% since 1975 (Commane *et al* 2017). These observed increases in soil respiration  
4 have been attributed to increased ground thaw (Kim *et al* 2006) and residual unfrozen water in  
5 soil pore space (Faucherre *et al* 2018). Further, a recent synthesis of soil flux indicated soil  
6 respiration from Arctic-boreal permafrost regions may already outweigh ecosystem CO<sub>2</sub> uptake  
7 under contemporary climate conditions (Natali & Watts *et al* 2019).  
8  
9 109

110 Little is known about the spatiotemporal patterns of soil CO<sub>2</sub> emissions from tundra and  
111 boreal biomes at the regional level, in part due to the lack of spatial representation by in situ  
112 observations. Existing in situ (e.g., EC) and satellite-based CO<sub>2</sub> monitoring networks are unlikely  
113 to detect changes in soil respiration across the permafrost domain (Parazoo *et al* 2016),  
114 especially in winter months, or identify local changes in net ecosystem exchange (NEE) or  
115 component (i.e., GPP and respiration) CO<sub>2</sub> fluxes (Schimel *et al* 2015).  
116

117 Process-based terrestrial models can be useful tools to diagnose how components of the  
118 carbon cycle might change in response to shifts in ecosystem properties and climate but are  
119 hampered in representing seasonal and spatial patterns by the lack of integrated observations  
120 (Fisher *et al* 2018, Natali & Watts *et al* 2019). In many regions, including Northern Eurasia and  
121 Alaska, process-models have failed to agree on flux magnitudes and even the sink vs. source  
122 status of ecosystem carbon budgets (Fisher *et al* 2014, Rawlins *et al* 2015). Improving process-  
123 level understanding of soil respiration requires integrating in situ flux data, observations of  
124 ecosystem properties (e.g., vegetation characteristics, thermal and moisture state) from satellite  
125 remote sensing, and data-informed modeling (Jeong *et al* 2018, Schimel *et al* 2019).  
126

127 This study addresses knowledge gaps in our understanding of soil respiration from  
128 permafrost ecosystems. We seek to improve understanding of the spatiotemporal patterns of soil  
129 respiration in boreal and tundra landscapes, the magnitudes of seasonal and annual soil CO<sub>2</sub> loss,  
130 and how soil respiration impacts ecosystem carbon budgets. Here we apply information gained  
131 from a new network of Soil Respiration Stations (SRS) within the NASA Arctic Boreal  
132 Vulnerability Experiment (ABOVE) domain. We also incorporate a complementary suite of flux  
133 records from EC towers within the region. We used Random Forest models and remote sensing  
134 to extrapolate soil fluxes to the ABOVE domain for the 2016-2017 period, obtaining spatially and  
135 seasonally disaggregated regional estimates of soil emissions. Last, we determine the seasonal  
136  
137  
138  
139  
140  
141  
142  
143  
144  
145  
146  
147  
148  
149  
150  
151  
152  
153  
154  
155  
156  
157  
158  
159  
160

1  
2  
3 134 and annual offset of GPP by respiration (soil, and ecosystem) to identify landscape net annual  
4  
5 135 carbon source, or sink, status under contemporary climate conditions.  
6  
7  
8 136 **2. Methods**  
9  
10  
11 137 *2.1. Study region*  
12  
13 138 The spatial domain of this study, which includes permafrost-affected landscapes of Alaska and  
14  
139 Northwest Canada, represents the core region of the NASA ABoVE Field Campaign (Kasischke  
15  
140 *et al* 2014, Loboda *et al* 2019) and spans gradients of climate, permafrost distribution (or  
16  
141 prevalence), vegetation, and ecosystem disturbance from fires (Figure 1). Approximately 24% of  
17  
142 the region has been recently burned (between 2000 and 2017; Loboda *et al* 2017a, 2017b,  
18  
143 Pastick *et al* 2018). Because our flux sampling locations only represent permafrost-affected  
19  
144 ecosystems, our analyses excluded landscapes where permafrost was absent (Gruber 2012); we  
20  
145 also excluded barren lands (< 10% vegetation) and open water.  
21  
22  
23 146 *2.2. SRS chamber data*  
24  
25 147 We used CO<sub>2</sub> flux data from 10 SRS (Minions *et al* 2019) installed along a north-south gradient  
26  
27 in Alaska, spanning the North Slope to Eight Mile Lake near Denali National Park (Figure 1;  
28  
29 148 *Supporting Information, SI Table 1*). Each SRS is a fully automated system that measures soil  
30  
31 149 surface CO<sub>2</sub> flux using three forced diffusion (FD) chambers. The SRS technique was designed  
32  
33 150 to provide year-round measurements of soil emissions (live aboveground vegetation was  
34  
35 151 removed during chamber installations to ensure that flux measurements do not reflect net CO<sub>2</sub>  
36  
37 152 exchange), even during periods of snow cover. Detailed information about the SRS system and  
38  
39 153 FD processing is provided in the Supplement (*SI Section 1*). In addition to the SRS records,  
40  
41 154 chamber-based fluxes collected using an Eosense eosFD portable sensor near Council, Alaska  
42  
43 155 were obtained from project partners. Six of the 11 FD stations (SRS and the eosFD site) are in  
44  
45 156 tundra and five in the boreal region. Six of the SRS sites represent paired burned and unburned  
46  
47 157 ecosystems (*SI Table 1*).  
48  
49  
50  
51  
52  
53  
54  
55  
56  
57  
58  
59  
60

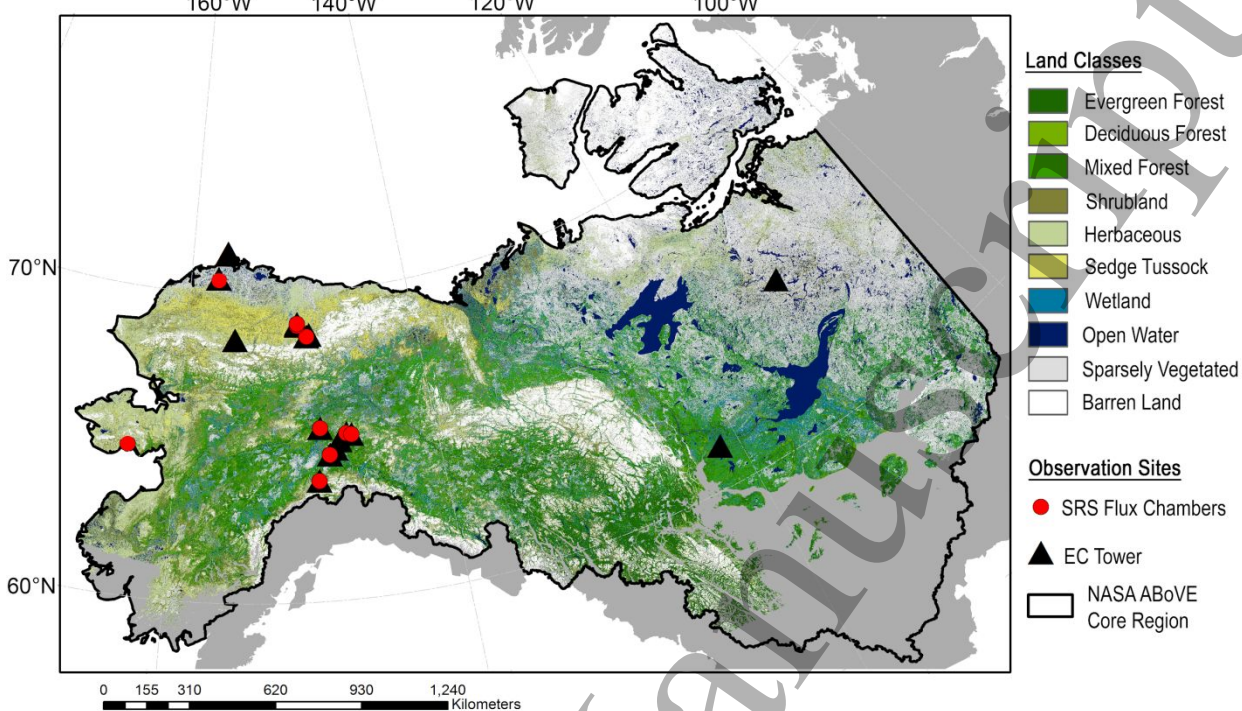


**Figure 1.** Locations of soil respiration stations (SRS) and eddy covariance (EC) towers considered in this study. The study domain is part of the NASA ABoVE core region. The sites span climate and vegetation gradients (tundra to boreal) within Alaska and Northwest Canada. Landscapes evaluated in this study ( $2.68E12 \text{ km}^2$ ) do not include barren land, open water, or where permafrost was absent (indicated in grey). Landcover classes are from Wang *et al* (2019).

### 2.3. EC tower data

We used AmeriFlux ([ameriflux.lbl.gov](http://ameriflux.lbl.gov)) and EC-investigator provided quality-controlled  $\text{CO}_2$  flux records primarily from September 2016 through August 2017 (matching the period of highest data availability from the SRS sites) from 15 EC towers (Figure 1, see *SI Table 1, SI Section 2.1*); 8 tower sites were in tundra and 7 in boreal. The half hourly EC records included NEE, GPP, and ER. NEE was obtained directly from the EC records and indicates the net of ecosystem  $\text{CO}_2$  respiration and  $\text{CO}_2$  uptake; GPP and ER were obtained using standard EC flux partitioning algorithms (Reichstein *et al* 2005, Lasslop *et al* 2010). Quality data were available year-round for at least ten sites (*SI Table 1; SI Figure 2*).

### 2.4. Flux modeling

We used published values from field and laboratory studies to separate aboveground respiration components from the EC-based ER records (*SI Section 2.2*). We acknowledge that the literature-based ratio approach does not account for seasonal variability in aboveground respiration, and

1  
2  
3 178 variability from other factors including temperature, species type, total biomass, and ecosystem  
4 179 stress. However, this approach was used because more detailed information was not available.  
5 180 We then used the combined SRS FD and EC ER dataset, information from remote sensing, and  
6 181 ancillary geospatial layers (*SI Section 3*) to obtain data-driven Random Forest models (*SI Section*  
7 182 *4*) developed separately for summer (June – August), autumn (September, October), winter  
8 183 (November – March) and spring (April and May). These seasons were based on observed  
9 184 seasonality in the tundra and boreal SRS and EC flux records (*SI Figure 3*). Candidate variables  
10 185 used in the models are described in the Supplement (*SI Section 3*) and included information  
11 186 about vegetation greenness and productivity, leaf area, topography, soil characteristics (e.g.,  
12 187 permafrost status, soil texture, soil organic carbon content), and other environmental conditions  
13 188 (e.g., albedo, radiation, temperature, snow cover, soil moisture status).  
14  
15  
16  
17  
18  
19  
20  
21  
22  
23  
24  
25  
26  
27  
28  
29  
30  
31  
32  
33  
34  
35  
36  
37  
38  
39  
40  
41  
42  
43  
44  
45  
46  
47  
48  
49  
50  
51  
52  
53  
54  
55  
56  
57  
58  
59  
60

#### 189 *2.4.1 Random forest models and spatial prediction*

190 Random Forest (RF) is a machine learning method that uses an ensemble approach to regression  
191 by means of multiple decision trees and bootstrap sampling (Liaw & Wiener 2002, Cutler *et al*  
192 2012). RFs have been widely used in ecological studies (Pearson *et al* 2013, Clewley *et al* 2017)  
193 and carbon budget assessments (Tramontana *et al* 2015, Jung *et al* 2020). Strengths of RF  
194 include the ability to handle high-dimensional problems, noise, and non-linearity, and its ability  
195 to provide robust internal estimates of error and variable importance (Cutler *et al* 2012).

196 We developed RF models in the R computing environment (R Core Team 2019) using the  
197 randomForest package (Liaw 2018). Each tree was constructed using a random selection (i.e.,  
198 bagging) of approximately 2/3 of the samples (42 site-flux observations in the autumn model,  
199 110 in the winter model, 48 in the spring model and 65 in the summer model; see *SI Section 4.1*).  
200 The remaining 1/3 of the observations was used to validate each tree in the forest (1000 trees per  
201 trained RF model). Predictor variable (*SI Table 4*) selection was achieved using the Variable  
202 Selection Using Random Forest (VSURF; Genuer *et al* 2019, Genuer *et al* 2010) R package  
203 which was designed to reduce high (>70%) cross-correlations between the selected inputs. The  
204 tuneRF algorithm (Liaw 2018) was applied to optimize the Mtry parameter (the number of  
205 variables available for splitting at each tree node). Variable importance was assessed using  
206 randomForest varImpPlot (Liaw 2018) and the rfPermute (Archer 2020) R package was used to  
207 provide corresponding estimates of parameter significance. This process was applied to obtain

optimal RF models for each season (*SI Section 4.2*). The final models were applied to the raster predictor datasets (raster package in R; Hijmans *et al* 2020) to obtain 300-m resolution maps of monthly average soil respiration.

### 2.4.2 ABoVE region carbon budgets

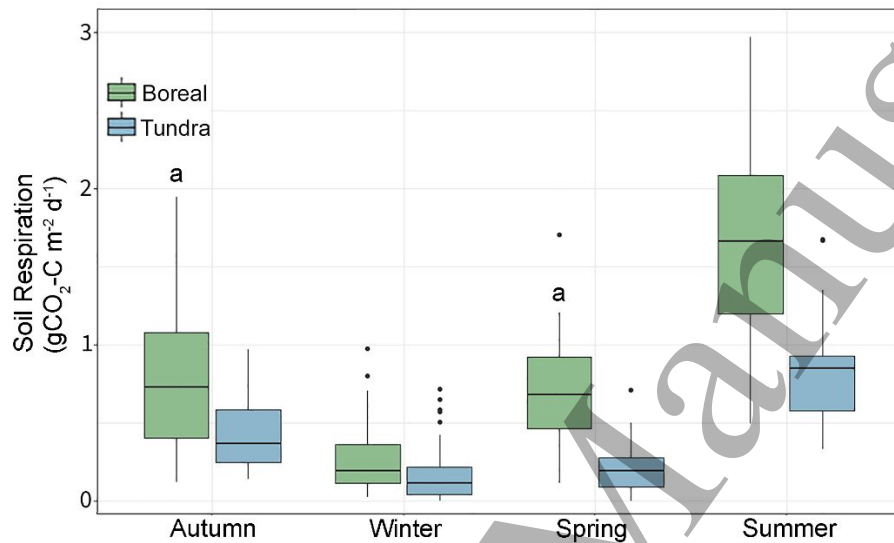
We used the monthly average soil CO<sub>2</sub> emission maps (gCO<sub>2</sub>-C m<sup>-2</sup> d<sup>-1</sup>) from the RF models to obtain regional flux budgets. The emission estimates were scaled to the terrestrial spatial domain within each 300 x 300 m grid cell by removing fractions of identified open water within each grid cell. Fractional water was derived using the 30-m Wang *et al* (2019) land cover map for 2014. We then obtained monthly and annual soil respiration totals for the ABoVE domain (T<sub>g</sub> CO<sub>2</sub>-C period<sup>-1</sup>). To determine the extent that soil respiration offset the annual ecosystem uptake of CO<sub>2</sub> (i.e., GPP), we obtained estimates from an ensemble of satellite observation based GPP records for the 2016 and 2017 period (*SI Section 3*), including NASA MODIS MOD17 (MOD17A2H.006, Running *et al* 2015), NASA Soil Moisture Active Passive (SMAP) Level 4 Carbon (L4\_C) (Kimball *et al* 2014, Jones *et al* 2017) and Global OCO-2 SIF (GOSIF) GPP data products (Li & Xiao 2019). Lastly, to gauge the potential impact of regional NEE on annual GPP, we used literature-based flux ratios (*SI Section 2*) to provide estimates of emissions from aboveground respiration, in addition to our RF-estimates of soil respiration.

### 3. Results

### *3.1 Soil emission characteristics*

227 Site-level fluxes showed strong seasonal emission patterns (Figure 2) closely tied to changes in  
 228 air and soil temperature (Figure 3). Soil respiration (regional mean  $\pm$  standard deviation) was  
 229 largest in summer (boreal:  $1.87 \pm 0.67$  gCO<sub>2</sub>-C m<sup>-2</sup> d<sup>-1</sup>; tundra:  $0.94 \pm 4$  gCO<sub>2</sub>-C m<sup>-2</sup> d<sup>-1</sup>) and  
 230 peak daily-averaged respiration was often observed in July (*SI Figure 3*), the warmest month (air  
 231 temperatures  $> 10$  °C, at EC and SRS flux sites). This was followed by a steady decline in  
 232 autumn (boreal:  $0.8 \pm 0.4$  gCO<sub>2</sub>-C m<sup>-2</sup> d<sup>-1</sup>; tundra:  $0.42 \pm 0.2$  gCO<sub>2</sub>-C m<sup>-2</sup> d<sup>-1</sup>). Winter respiration  
 233 persisted even under snow cover, and cold air and soil (10-15 cm depth) temperatures averaging  
 234  $-18 \pm 6$  °C and  $-3.5 \pm 2.7$  °C, respectively. In winter, boreal soil respiration averaged  $0.24 \pm 0.2$   
 235 gCO<sub>2</sub>-C m<sup>-2</sup> d<sup>-1</sup> and tundra averaged  $0.18 \pm 0.16$  gCO<sub>2</sub>-C m<sup>-2</sup> d<sup>-1</sup>. Soil respiration began to  
 236 increase again in spring (boreal:  $0.82 \pm 0.6$  gCO<sub>2</sub>-C m<sup>-2</sup> d<sup>-1</sup>; tundra:  $0.28 \pm 0.2$  gCO<sub>2</sub>-C m<sup>-2</sup> d<sup>-1</sup>) as  
 237 ecosystems warmed (average boreal/tundra soil temperatures of  $-1.98$  °C in April,  $-0.07$  °C in

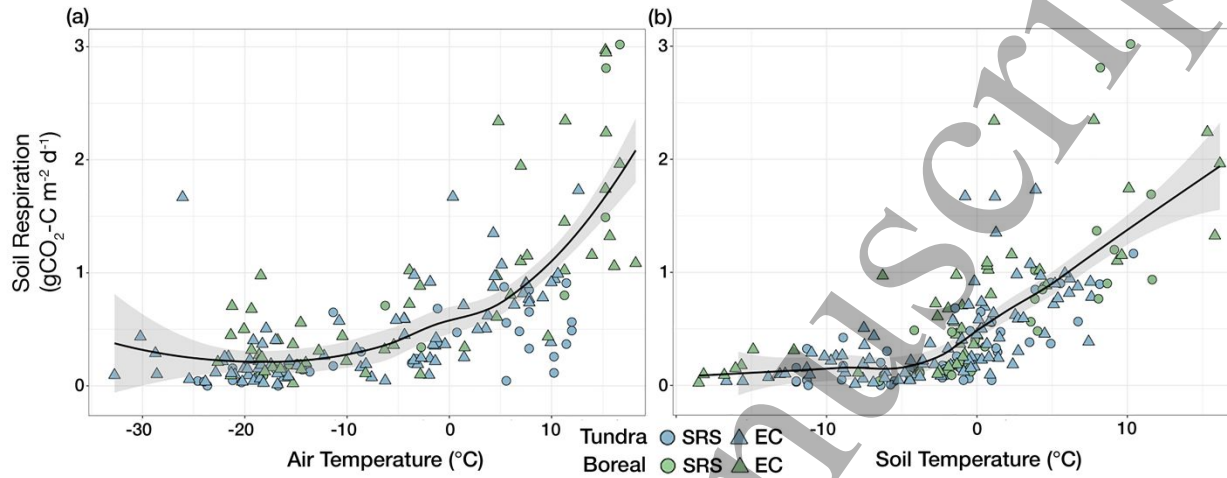
1  
2  
3 238 May, and 1.82 °C in June). Soil respiration from boreal sites was systematically higher than  
4 those from tundra in all seasons, excluding winter (t-test;  $p=0.03$  in autumn,  $p=0.22$  in winter,  
5  $p=0.002$  in spring,  $p < 0.001$  in summer). T-test significance for monthly flux averages is shown  
6 in *SI Figure 3* and seasonal flux patterns according to biome (i.e., tundra or boreal) and flux  
7 location are shown in *SI Figure 4*.  
8  
9 242  
10 243



31 244  
32 245 **Figure 2.** Seasonal soil respiration patterns observed in the SRS and EC fluxes for the ABove  
33 246 domain, for boreal (green) and tundra (blue) biomes. Soil respiration emissions are average  
34 247 monthly fluxes from individual sites, totaling 45 site-fluxes in autumn, 110 in winter, 48 in  
35 248 spring, and 65 in summer. The boxplot range indicates the first and third quartiles; the middle  
36 249 line denotes the median. Box whiskers indicate minimum and maximum values, excluding  
37 250 outliers indicated by black circles; 'a' denotes t-test results with no significant difference  
38 251 between seasons at  $\alpha = 0.05$ .  
39 252

40 253 Air temperature ( $p = 0.009$ ) and soil temperature at 10-15 cm depth ( $p = 0.01$ ) explained 65%  
41 of the observed variability in monthly soil respiration at the site level, in a linear regression  
42 analysis that included fluxes from all seasons. During the 2016-2017 period, soil respiration was  
43 observed even at air temperatures approaching -30 °C and at soil temperatures (~ 15 cm depth)  
44 below -10 °C (Figure 3a, b; *SI Figure 5*). Soil respiration increased steadily after ground thaw.  
45  
46 257 Soil respiration for the 14 tundra and boreal sites where in situ soil moisture was available  
47 indicated that higher fluxes in summer most often occurred where soils ( $\leq 15$  cm depth) were  
48 relatively wet but not saturated (*SI Figure 6*). Observed relationships between the seasonal site-  
49  
50 258  
51 259  
52 260

1  
2  
3 261 level soil respiration fluxes and important remote-sensing based indicators of permafrost status,  
4 262 temperature, soil moisture, and GPP is provided in *SI Figure 7*.  
5  
6  
7



263  
264 **Figure 3.** Observed relationships between (a) air temperature or (b) in situ soil temperature (  
265  $\sim 10\text{--}15 \text{ cm depth}$ ) and average monthly soil respiration ( $\text{gCO}_2\text{-C m}^{-2} \text{d}^{-1}$ ) from eddy covariance  
266 (EC; triangles) and soil respiration stations (SRS; circles) in Alaska and Northwest Canada for  
267 boreal (green) and tundra (blue) sites. Fitted curves (black lines) were obtained using locally  
268 weighted loess smoothing; grey shading represents confidence intervals (+/- standard error).

### 3.2 RF model performance and variable importance

270 The RF models explained much of the variance in soil respiration, with moderate-to-low root  
271 mean squared error (RMSE) and mean absolute error (MAE; *SI Table 5*, *SI Figure 8*). The  $R^2$   
272 values were 0.68 for the summer model, 0.57 for autumn, 0.65 for winter, and 0.76 for spring.  
273 The respective RMSE ( $\text{gCO}_2\text{-C m}^{-2} \text{d}^{-1}$ ) values were 0.35 (summer), 0.24 (autumn), 0.10  
274 (winter), and 0.25 (spring). The positive MAE (averaging  $0.2 \pm 0.09 \text{ gC m}^{-2} \text{d}^{-1}$ ) indicated a  
275 slight underestimation of soil respiration by the models. In the summer RF model, MODIS  
276 (MOD) GPP was the most important variable, followed by soil sand content (an indicator of  
277 water retention and nutrient content), MODIS leaf area index (LAI), tree cover, and normalized  
278 difference vegetation index (NDVI; an indicator of greenness). In the autumn model, SMAP  
279 Root Zone Soil Moisture (RZSM) was the most important predictor (Table 1), followed by  
280 permafrost zonation index (PZI), SMAP soil temperature (TSOIL) from layer 4 (70-140 cm  
281 depth), downwelling shortwave radiation (RAD), and SoilGrids SOC (0-30 cm depth). In winter,  
282 the Landsat-based Normalized Difference Water Index (NDWI; an indicator of landscape  
283 wetness gradients) was most important, providing finer resolution (30-m) legacy information

1  
2  
3 284 about moisture status from the previous summer. Other significant predictors were MODIS LAI,  
4 Landsat enhanced vegetation index (EVI; another indicator of greenness), SMAP RZSM, PZI, a  
5 MODIS snow index (NDSI), and SMAP layer 3 (~30-70 cm) TSOIL. The 30-70 cm soil  
6 temperature selected by the winter model may better represent the delay in active-layer freeze as  
7 deeper soils remain closer to 0 °C even after upper-layers have frozen (e.g., Zona *et al* 2016).  
8 The PZI was the most important variable for the spring model, followed by tree cover, land  
9 surface temperature (LST), soil clay content, MODIS GPP, Landsat EVI, and SMAP surface (0-  
10 10 cm) soil moisture (SM).  
11  
12  
13  
14  
15  
16  
17  
18 292 **Table 1.** Variable importance for the seasonal RF models, according to the percentage increase  
19 in model mean squared error (%IncMSE) when a specific variable was excluded in the  
20 development of regression trees. Larger values for %IncMSE indicate greater importance of the  
21 predictor variable relative to the other predictors. MON indicates that variable information was  
22 input for each month and Summer indicates variable information from June-August.  
23

Summer			Autumn		
Variable	%IncMSE	p-value	Variable	%IncMSE	p-value
MOD GPP (Summer)	22.02	0.0033	SMAP RZSM (MON)	19.83	0.0016
SoilGrids % Sand	21.52	0.0033	PZI	16.32	0.0033
MOD LAI (Summer)	20.24	0.0003	SMAP Tsoil L4 (MON)	15.69	0.0017
MOD % Tree Cover	20.23	0.0050	SMAP RAD (MON)	15.43	0.0049
MOD NDVI (MON)	17.60	0.0067	SoilGrids SOC	9.44	0.0549
Winter			Spring		
Variable	%IncMSE	p-value	Variable	%IncMSE	p-value
Landsat NDWI (Summer)	22.53	0.0017	PZI	17.47	0.0019
MOD LAI (Summer)	21.14	0.0016	MOD % Tree Cover	16.94	0.0009
Landsat EVI (Summer)	21.13	0.0017	MOD LST (MON)	12.79	0.1798
SMAP RZSM (MON)	20.79	0.0016	SoilGrids % Clay	12.67	0.0099
MOD GPP (Summer)	19.78	0.0017	MOD GPP (Summer)	12.05	0.0079
PZI	18.85	0.0017	Landsat EVI (Summer)	10.40	0.0159
MOD NDSI (MON)	18.11	0.0016	SMAP SM (Summer)	10.12	0.0229
SMAP TSOIL L3 (MON)	10.70	0.0233			

297

298

299

300

301

302

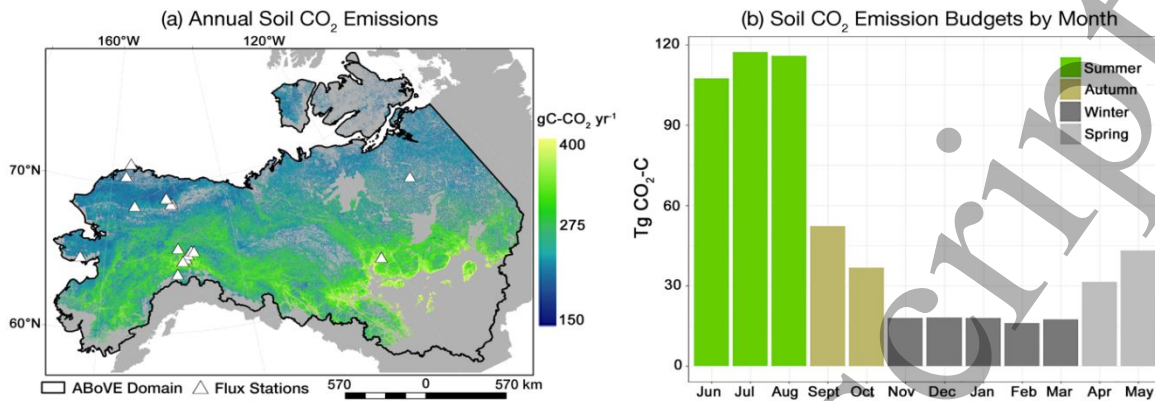


Figure 4. (a) Annual soil respiration emissions ( $\text{gCO}_2\text{-C m}^{-2}$ ) per 300-m grid cell for the ABoVE domain (2016-2017). Estimates exclude non-permafrost, barren, and open water (in grey) areas. Triangles indicate EC and SRS flux monitoring sites used for model development. (b) Monthly RF-derived respiration ( $\text{TgCO}_2\text{-C}$ ) for the ABoVE region.

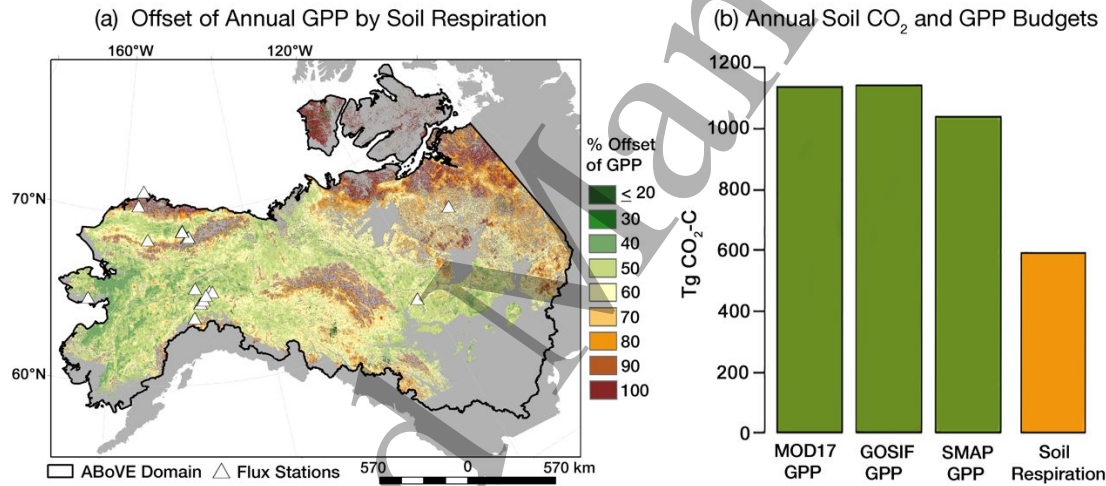


Figure 5. (a) Reduction (offset) of GPP by soil respiration. A 100% offset indicates that soil respiration equaled or exceeded GPP. Triangles indicate CO<sub>2</sub> flux monitoring stations (EC and SRS) used for model development. (b) Annual soil respiration and GPP totals ( $\text{TgCO}_2\text{-C}$ ) for the ABoVE domain. GPP is from MODIS (MOD17), GOSIF, and SMAP L4\_C products.

### 3.3 Annual carbon flux estimates for ABoVE domain

Annual soil respiration emission for the study domain was  $591.2 \text{ TgC-CO}_2 \pm 120 \text{ TgC-CO}_2$  during the 2016-2017 period (Figure 4; SI Table 6). Monthly soil respiration maps are provided in SI Figure 9 and seasonal respiration budgets are shown in SI Figure 10 (SI Figure 11 shows associated emission uncertainty maps). Summer (June – August) contributed to 58% of annual soil respiration, the longer winter (November – March) period generated 15%, with comparable proportions occurring in autumn (15%, September, October) and spring (12%, April, May). Across the ABoVE region, the largest soil respiration budgets occurred in the boreal zones and

321 the warmer, more southern, forest-tundra ecotone. Over half of regional soil respiration  
 322 emissions (54% of annual total) were from colder landscapes having a widespread occurrence of  
 323 near-surface permafrost (i.e., where the PZI was  $> 75\%$ ; spanning 70% of the domain) and the  
 324 remaining 46% of emissions were from warmer permafrost ( $0\% < \text{PZI} > 75\%$ ; 30% of the  
 325 domain; Table 2; *SI Figure 12*). The area covered by Shrubland/Herbaceous vegetation produced  
 326 the majority (46%) of soil respiration, followed by Sparse Vegetation and Evergreen Forest.

327 **Table 2.** Percent of annual soil respiration and annual GPP totals for the study domain,  
 328 according to tundra (including shrub tundra and excluding transitional tundra-boreal biomes) and  
 329 boreal biomes (from Natali & Watts *et al* 2019), vegetation cover (from Wang *et al* 2019) and  
 330 permafrost class (Gruber *et al* 2019).

Land Cover	% of Domain	% of GPP	% of Soil Respiration
Boreal Biome	86	85	83
Tundra Biome	14	15	17
Shrubland/Herbaceous	43.7	49	46
Sparse Vegetation	22.9	17	19
Evergreen Forest	14.3	15	16
Wetland	10.4	10	10
Mixed Forest	3.3	4	3.5
Tussock Tundra	3.7	3	2.9
Deciduous Forest	1.7	2	2.6
Permafrost Class	% of Domain	% of GPP	% of Soil Respiration
PZI $> 75$	70	38	54
$50 < \text{PZI} \leq 75$	14	21	12
$25 < \text{PZI} \leq 50$	9	21	8
$0 < \text{PZI} \leq 25$	7	20	26

331 Annual GPP for the whole domain, obtained from MOD17, GOSIF, and SMAP L4\_C  
 332 products (Section 2.4.2, *SI Figure 13*), was 1046-1256 TgCO<sub>2</sub>-C in 2016 and 1025-1134 TgCO<sub>2</sub>-  
 333 C in 2017 (*SI Table 7*) with an estimated uncertainty of 310 TgCO<sub>2</sub>-C yr<sup>-1</sup> (*SI Section 3*). Annual  
 334 GPP was considerably higher ( $> 600 \text{ gCO}_2\text{-C m}^{-2} \text{ yr}^{-1}$ ) in the boreal regions relative to tundra ( $<$   
 335 300 gCO<sub>2</sub>-C m<sup>-2</sup> yr<sup>-1</sup>; *SI Figure 13*). Our extrapolations indicate soil respiration offset  
 336 approximately 54% of GPP across the domain (averaging 1101 TgCO<sub>2</sub>-C). The offset of GPP by  
 337 soil respiration varied considerably across the region (Figure 5; *SI Figure 14*). Offsets of  $\geq$   
 338 100% (i.e., annual net carbon source areas) were identified in far northern tundra and  
 339 mountainous landscapes, along transitional tundra-boreal ecotones, and in landscapes recently  
 340 disturbed by fire (e.g., west of Hudson Bay & south of the Selwyn Mountains in Canada). We  
 341 estimate that approximately 8% of the ABoVE region was a net carbon source (100% offset of

1  
2  
3 342 GPP) in 2016-2017, based on soil respiration alone and not accounting for aboveground  
4 respiration and non-terrestrial carbon emissions (i.e., aquatic bodies).  
5  
6

7 344 **4. Discussion**  
8  
9

10 345 This study provides new estimates of soil respiration for the ABoVE domain and insights into  
11 how soil respiration is offsetting net annual GPP across permafrost-affected tundra and boreal  
12 landscapes. Our analysis of in situ observations and RF-model results indicate that soil  
13 respiration was generally highest under warmer (above freezing) soil temperatures and deeper  
14 seasonal soil thaw, in moderate-to-moist soils (0.5-0.8 m<sup>3</sup> m<sup>-3</sup>), and in areas with higher  
15 vegetation productivity. Accordingly, the largest annual soil respiration rates occurred in boreal  
16 ecosystems where trees and shrubs were present, especially along the more southern portions of  
17 the domain with substantial permafrost thaw.  
18  
19

20 353 *4.1 The temperature-soil respiration relationship*  
21  
22

23 354 Consistent with earlier studies (e.g., Wickland *et al* 2006, Natali *et al* 2014, Loranty *et al*  
24 355 2018), we found temperature to be an important driver of soil respiration at the site level. Our  
25 356 regional flux assessments showed highest soil respiration rates in summer (contributing to 58%  
26 357 of annual soil respiration) when soil temperatures were warmer and soil thaw was deepest.  
27 358 Higher emissions in warmer soils are not only from increased microbial decomposition of SOC,  
28 359 but likely also from increased root activity (i.e., belowground autotrophic respiration), a strong  
29 360 source of CO<sub>2</sub> in thawing permafrost systems (Hicks Pries *et al* 2015, 2016). Although gridded  
30 361 estimates of belowground root density are not available for this region, LAI, % tree cover, and  
31 362 vegetation indices (important predictors in the RF models) provided proxies of vegetation  
32 363 productivity (e.g., Street *et al* 2006), and indirect information about root respiration.  
33  
34

35 364 Within the site-level soil respiration database, larger, and sometimes episodic, CO<sub>2</sub> emissions  
36 365 (> 0.5 gCO<sub>2</sub>-C m<sup>-2</sup> d<sup>-1</sup>) were observed as soil temperatures approached 0 °C, especially as soil  
37 366 layers began to freeze in the autumn. Like our site-level findings, an atmospheric study of  
38 367 Alaska's North Slope also identified high CO<sub>2</sub> emissions in autumn and early winter (October –  
39 368 December; Commane *et al* 2017) during the landscape freeze. Although our RF model approach  
40 369 represented regional flux characteristics relatively well, the autumn RF model had the lowest  
41 370 performance of the four seasonal models, resulting from its inability to capture spatiotemporally  
42  
43

1  
2  
3 371 episodic releases of CO<sub>2</sub> observed in situ. As a result, the model underestimated regional CO<sub>2</sub>  
4 372 emissions (by  $\geq 0.2$  gC m<sup>-2</sup> d<sup>-1</sup>, based on MAE estimates) during the autumn period.  
5  
6 373  
7  
8 374 *4.2 Regional predictors of soil respiration*  
9

10 375 Our regional assessments show that carbon source/sink status is highly heterogeneous.  
11 376 Annual carbon status of an ecosystem is influenced by many factors, including GPP and plant  
12 377 community type (e.g., Rouse *et al* 2002, Parmentier *et al* 2011, Oechel *et al* 2014, Forkel *et al*  
13 378 2016, Ge *et al* 2017, Christiansen *et al* 2018), winter snow cover which insulates soils (e.g.,  
14 379 Welker *et al* 2000, Christiansen *et al* 2018), and shifts in vegetation growth and microbial  
15 380 activity (Arndt *et al* 2019, Kim *et al* 2021). Soil moisture is also an extremely influential factor  
16 381 that is very heterogeneous across the landscape and affects both vegetation productivity and soil  
17 382 respiration (Grogan & Chapin III 1999), yet this environmental variable can be radically altered  
18 383 by permafrost thaw (Jorgenson *et al* 2013) and is especially difficult to monitor regionally at  
19 384 finer landscape-level scales (Du *et al* 2019).  
20  
21

22 385 Burn status (i.e., burned or unburned) was not a significant predictor of the regional monthly-  
23 386 averaged soil respiration emissions examined in this analysis, which could be in part due to our  
24 387 database containing information from only three burn sites (representing tundra and forest  
25 388 landscapes 11-15 years after fire), or because of rapid post-fire recovery. Following a fire event,  
26 389 the combination of warmer and drier soils can substantially increase CO<sub>2</sub> flux from soils (O'Neill  
27 390 *et al* 2002, 2003, Ueyama *et al* 2019). However, a review of fire disturbance at high latitudes  
28 391 reported that soil and root respiration in forests may stabilize after a decade (Ribeiro-Kumara *et*  
29 392 *al* 2020). As a result, our estimates likely underestimate soil respiration from recently burned  
30 393 areas ( $\sim 5\%$  of the domain from 2012-2016; *SI Figure 15*; Alaska and Canada Large Fire  
31 394 Databases; Kasischke *et al* 2002, Amiro *et al* 2001, Stocks *et al* 2002).  
32  
33

34 395 *4.3 Regional carbon budgets*  
35  
36

37 396 Our 2016-2017 assessment shows an annual soil respiration loss of 591Tg CO<sub>2</sub>-C for the  
38 397 permafrost-affected ABoVE domain. A comparison of our RF-based results with the Natali &  
39 398 Watts *et al* (2019) pan-Arctic estimates (referred to as NCC 2019 and subset to the ABoVE  
40 399 permafrost-affected study area) showed that soil respiration estimates in the NCC 2019 record  
41 400 was substantially higher ( $\sim 1.6x$ ) than our RF budgets during the winter and early spring (*SI*  
42  
43  
44  
45  
46  
47  
48  
49  
50  
51  
52  
53  
54  
55  
56  
57  
58  
59  
60

1  
2  
3 401 *Table 6 and SI Figure 16*). A corresponding model analysis by Schiferl *et al* (In Review) used a  
4 402 Stochastic Time-Inverted Lagrangian Transport (STILT; Lin *et al* 2003) model and atmospheric  
5 403 CO<sub>2</sub> observations influenced by Alaska North Slope tundra (obtained from the Utqiagvik tall  
6 404 tower) to verify the NCC 2019 and RF-model results. The study determined that our RF-model  
7 405 approach underestimated atmospheric enhancements in October-December by 2-3x but the RF-  
8 406 estimates were much better aligned with atmospheric observations, relative to NCC 2019, during  
9 407 the January-April period (*SI Section 5, SI Figure 17*). While episodic bursts of CO<sub>2</sub> from  
10 408 freezing soils may contribute to the larger atmospheric CO<sub>2</sub> levels observed October-December  
11 409 across the North Slope, our assessments also indicate that very large emissions of CO<sub>2</sub> to the  
12 410 atmosphere could result from the turnover and freeze of lakes and ponds which are widespread  
13 411 throughout the region (*SI Section 5*; Preskienis *et al* 2021). If this assessment is correct, then the  
14 412 Natali & Watts *et al* (2019) results also overestimate soil CO<sub>2</sub> emissions for the North Slope  
15 413 during the autumn season.  
16  
17

18 414 For the ABoVE study domain in 2016-2017, soil respiration only partially offset GPP, by  
19 415 approximately 54% to 60%. However, for many grid cells in northern tundra, mountainous  
20 416 regions, or where boreal forest GPP was reduced by recent fire (*SI Figure 14, 15*) soil respiration  
21 417 alone (not accounting for aboveground autotrophic respiration) equaled or exceeded annual GPP,  
22 418 indicating that some sites are net CO<sub>2</sub> sources. The Belshe *et al* (2013) meta-analysis of EC  
23 419 fluxes from high-latitude tundra sites concluded that tundra systems are currently CO<sub>2</sub> sources.  
24 420 Similarly, Natali & Watts *et al* (2019) determined the permafrost-affected Arctic-boreal zone to  
25 421 likely be a net CO<sub>2</sub> source when considering winter contributions from soils. Using published  
26 422 ratio estimates of aboveground vs belowground (soil) contributions to ER for boreal and tundra  
27 423 biomes we estimate an annual ER between 820 and 1171 Tg CO<sub>2</sub>-C, respectively offsetting 74-  
28 424 106% of annual GPP (*SI Figure 18*). This estimate suggests that tundra is currently a CO<sub>2</sub> source,  
29 425 while the boreal is a CO<sub>2</sub> sink.  
30  
31

## 32 426 **5. Conclusion**

33 427 Soil respiration can strongly impact the carbon sink or source status of high latitude permafrost  
34 428 regions. When considering the permafrost-affected tundra and boreal biomes of Alaska and  
35 429 Northwest Canada as a whole, soil respiration offset annual GPP in 2016-2017 by 54-60%.  
36 430 However, in sparsely vegetated tundra regions and recently burned landscapes, soil respiration  
37 431 exceeded GPP. Although a majority (58%) of annual soil respiration emissions occurred in the  
38  
39  
40  
41  
42  
43  
44  
45  
46  
47  
48  
49  
50  
51  
52  
53  
54  
55  
56  
57  
58  
59  
60

1  
2  
3 432 summer months, we found considerable contributions of soil CO<sub>2</sub> in the shoulder and winter  
4 433 seasons. Our soil emission estimate of  $\sim 591 \pm 120$  Tg CO<sub>2</sub>-C for the domain is likely  
5 434 conservative due to the inability of our statistical model approach to capture episodic bursts of  
6 435 CO<sub>2</sub> during soil freeze and thaw, and a lack of soil respiration data from very recent fire scars.  
7 436 We also acknowledge uncertainties introduced by using a simple literature-based flux correction  
8 437 ratio method to remove aboveground components from tower-based ER observations, which  
9 438 does not account for variability in aboveground respiration by species, temperature, stand age  
10 439 and other factors. We also note that the 2016-2017 period was characterized by record breaking  
11 440 high air temperatures across much of the region relative to previous years and the longer-term  
12 441 1981-2019 normal (ACRC 2016, 2017). Warming records have been repeatedly broken in more  
13 442 recent years and we estimate that post-2017 soil respiration budgets will exceed those reported  
14 443 here.  
15  
16  
17  
18  
19  
20  
21  
22  
23  
24

25 444 Our data-driven gridded soil respiration budgets provide new, valuable records that will be  
26 445 useful for the future benchmarking of process-based models. Although our assessment is limited  
27 446 to a one-year period, efforts to ensure the continued operation of SRS and EC sites will allow  
28 447 future regional studies to better understand interannual variability and spatiotemporal trends in  
29 448 soil respiration across the rapidly changing Arctic-boreal environment. As current spaceborne  
30 449 observations of CO<sub>2</sub> are not yet able to track changing emission contributions in winter, nor able  
31 450 to identify finer landscape-level patterns of soil emissions (Parazoo *et al* 2016), the continuation  
32 451 if not expansion of existing in situ monitoring networks is urgently needed to document changes  
33 452 in soil respiration and ecosystem carbon sink/source status across the thawing permafrost region  
34 453 in North America and elsewhere, including Siberia and the Tibetan Plateau.  
35  
36  
37  
38  
39  
40  
41  
42  
43  
44  
45  
46  
47  
48  
49  
50  
51  
52  
53  
54  
55  
56  
57  
58  
59  
60

### 455 Acknowledgements

456  
457 J.D.W., S.M.N. and S.J.G. acknowledge support from NASA ABoVE (NNX15AT81A;  
458 80NSSC19M0209); J.D.W. from the NASA New Investigator Program (NNH17ZDA001N);  
459 S.M.N., S.P. and J.D.W. from the Gordon and Betty Moore Foundation. Y.K. and B.Y.L. from  
460 the Korea Polar Research Institute (KOPRI, PN21081). J.X. and X.L. were supported by NASA  
461 Climate Indicators and Data Products for Future National Climate Assessments  
462 (NNX16AG61G). H.I., M.U, and H.K. were supported by the Japan MEXT ArCS II project  
463 (JPMXD1420318865) and M.U by the ArCS project (JPMXD1300000000). A.V.R. was  
464 supported by NSF LTREB grant #1556772 to the University of Notre Dame. E.A.G. Schuur  
465 recognizes support from the National Parks Inventory and Monitoring Program; National  
466 Science Foundation Bonanza Creek LTER program, Award #1026415; NNA LTREB: The  
467  
468  
469  
470  
471  
472  
473  
474  
475  
476  
477  
478  
479  
480  
481  
482  
483  
484  
485  
486  
487  
488  
489  
490  
491  
492  
493  
494  
495  
496  
497  
498  
499  
500  
501  
502  
503  
504  
505  
506  
507  
508  
509  
510  
511  
512  
513  
514  
515  
516  
517  
518  
519  
520  
521  
522  
523  
524  
525  
526  
527  
528  
529  
530  
531  
532  
533  
534  
535  
536  
537  
538  
539  
540  
541  
542  
543  
544  
545  
546  
547  
548  
549  
550  
551  
552  
553  
554  
555  
556  
557  
558  
559  
560

1  
2  
3 467 Arctic Carbon and Climate (ACCLIMATE) Observatory: Tundra Ecosystem Carbon Balance  
4 468 and Old Carbon Loss as a Consequence of Permafrost Degradation (Award #1754839). Special  
5 469 thanks to the NASA ABoVE logistics office for field activity support.  
6 470  
7 471

## 8 471 **Data availability statement**

9 473 Data from this study are included within the article and supplementary information and are  
10 474 available through the ORNL DAAC.  
11 475  
12 476

## 13 476 **References**

- 14 477  
15 478 ACRS 2016 Alaska Climate Summary. Alaska Climate Research Center Geophysical Institute,  
16 479 University of Alaska. Available at: <http://akclimate.org/Summary/2016/Annual>  
18 480 ACRS 2017 Alaska Climate Summary. Alaska Climate Research Center Geophysical Institute,  
19 481 University of Alaska. Available at: <http://akclimate.org/Summary/2017/Annual>  
21 482  
22 483 Arndt K A, Santos M J, Ustin S, Davidson S J, Stow D, Oechel W C, Tran T T P, Graybill B,  
23 484 and Zona D 2019 Arctic greening associated with lengthening growing seasons in Northern  
24 485 Alaska *Environmental Research Letters* **14** 145018.  
25 486 Amiro B D, Todd J B, Wotton B M, Logan K A, Flannigan K A, B J Stocks, *et al* 2001 Direct  
26 487 carbon emissions from Canadian forest fires *Canadian Journal of Forest Research* **31** 512-525.  
28 488 Baldocchi D D, Hincks B B, and Meyers T P 1988 Measuring biosphere-atmosphere exchanges  
29 489 of biologically related gases with micrometeorological methods *Ecology* **69** 1331-1340.  
31 490 Baldocchi D 2014 Measuring fluxes of trace gases and energy between ecosystems and the  
32 491 atmosphere – the state and future of the eddy covariance method *Global Change Biology* **20**  
33 492 3600-3609.  
34 493 Belshe E F, Schuur E A G, and Bolker B M 2013 Tundra ecosystems observed to be CO<sub>2</sub> sources  
35 494 due to differential amplification of the carbon cycle *Ecology Letters* **16** 1307-1315.  
37 495 Bond-Lamberty B, Wang C, and Gower S T 2004 A global relationship between the  
39 496 heterotrophic and autotrophic components of soil respiration? *Global Change Biology* **10** 1756-  
40 497 1766.  
41 498 Box J E, Colgan W T, Christensen T R, Schmidt N M, Lund M, Parmentier F-J W, Brown R,  
42 499 Bhatt U S, Euskirchen E S, and Romanovsky V E 2019 Key indicators of Arctic climate change:  
43 500 1971-2017 *Environmental Research Letters* **14** 045010.  
45 501 Christiansen C T, Lafreniere M J, Henry G H R, and Grogan P 2018 Long-germ deepened snow  
46 502 promotes tundra evergreen shrub growth and summertime ecosystem net CO<sub>2</sub> gain but reduces  
47 503 soil carbon and nutrient pools *Global Change Biology* **24** 3508-3525.  
49 504 Clewley D, Whitcomb J B, Akbar R, Silva A R, Berg A, Adams J R, Caldwell T, Entekhabi D,  
50 505 and Moghaddam M 2017 A method for upscaling in situ soil moisture measurements to satellite  
51 506 footprint scale using random forests *IEEE JSTARS* **10** 2663-2673.  
53 507 Commane R, Lindaas J, Benmergui J, Luus K A, Chang R Y-W, Daube B C, Euskirchen E S,  
54 508 Henderson J M, Karion A, Miller J B, *et al* 2017 Carbon dioxide sources from Alaska driven by  
55 509 increasing early winter respiration from Arctic tundra *PNAS* **114** 5361-5366.  
57  
58  
59  
60

- 1  
2  
3 510 Cutler A, Cutler D R, and Stevens J R 2012 Random forests. In: Zhang C., Ma Y (eds) *Ensemble*  
4 511 *Machine Learning*. Springer, Boston, MA.  
5  
6 512 Du J, Watts J D, Jiang L, Lu H, Cheng X, Duguay C, Farina M, Qiu Y, Kim Y, Kimball J S, and  
7 513 Tarolli P 2019 Remote sensing of environmental changes in cold regions: methods,  
8 514 achievements, and challenges *Remote Sensing* **16** 1952.  
9  
10 515 Faucherre S, Jorgensen C J, Blok D, Weiss N, Siewert M B, Bang-Andreasen T, Hugelius G,  
11 516 Kuhry P, and Elberling B 2018 Short and long-term controls on active layer and permafrost  
12 517 carbon turnover across the Arctic *JGR Biogeosciences* **123** 372-390.  
13  
14 518 Fisher J B, Sikka M, Oechel W C, Huntzinger D N, Melton J R, Koven C D, Ahlstrom A, Arain  
15 519 M A, Baker I, Chen J M, *et al* 2014 Carbon cycle uncertainty in the Alaskan Arctic  
16 520 *Biogeosciences* **11** 4271-4288.  
17  
18 521 Fisher J B, Hayes D J, Schwalm C R, Huntzinger D N, Stofferahn E, Schaefer K, Luo Y,  
19 522 Wullschleger S D, Goetz S, and Miller C E 2018 Missing pieces to modeling the Arctic-Boreal  
20 523 puzzle *Environmental Research Letters* **13** 020202.  
21  
22 524 Forkel M, Carvalhais N, Rodenbeck C, Keeling R, Heimann M, Thonicke K, Zaehle S, and  
23 525 Reichstein M 2016 Enhanced seasonal CO<sub>2</sub> exchange caused by amplified plant productivity in  
24 526 northern ecosystems *Science* **351** 696-699.  
25  
26 527 Gagnon S, Allard M, and Nicosia A 2018 Diurnal and seasonal variations of tundra CO<sub>2</sub>  
27 528 emissions in a polygonal peatland near Salluit, Nunavik, Canada *Arctic Science* **4** 1-15.  
28  
29 529 Ge L, Lafleur P M, and Humphreys E R 2017 Respiration from soil and ground cover vegetation  
30 530 under tundra shrubs *Arctic, Antarctic and Alpine Research* **49** 537-550.  
31  
32 531 Genuer R, Poggi J-M, and Tuleau-Malot C 2010 Variable selection using random forests *Pattern*  
33 532 *Recognition Letters* **31** 2225-2236.  
34  
35 533 Genuer R, Poggi J-M, and Tuleau-Malot C 2019 VSURF: Variable selection using random  
36 534 forests. Version 1.1.0. Available at: <https://github.com/robingenuer/VSURF>.  
37  
38 535 Grogan P, and Chapin III F S 1999 Arctic soil respiration: effects of climate and vegetation  
39 536 depend on season *Ecosystems* **2** 451-459.  
40  
41 537 Gruber S 2012 Derivation and analysis of a high-resolution estimate of global permafrost  
42 538 zonation *The Cryosphere* **6** 221-233.  
43  
44 539 Hadden D, and Grelle A 2016 Changing temperature response of respiration turns boreal forest  
45 540 from carbon sink to carbon source *Agricultural and Forest Meteorology* **223** 30-38.  
46  
47 541 Hermle S, Lavigne M B, Bernier P Y, Bergeron O, and Pare D 2010 Component respiration,  
48 542 ecosystem respiration and net primary production of a mature black spruce forest in northern  
49 543 Quebec *Tree Physiology* **30** 527-540.  
50  
51 544 Hicks Pries C E, van Logtestjin R S P, Schuur E A G, S M Natali, J H C Cornelissen, R Aerts,  
52 545 and Dorrepaal E 2015 Decadal warming causes a consistent and persistent shift from  
53 546 heterotrophic to autotrophic respiration in contrasting permafrost ecosystems *Global Change*  
54 547 *Biology* **21** 4508-4519.  
55  
56 548 Hicks Pries C E, Schuur E A G, Natali S M, and Crummer K G 2016 Old soil carbon losses  
57 549 increase with ecosystem respiration in experimentally thawed tundra *Nature Climate Change* **6**  
58 550 214-218.  
59  
60

- 1  
2  
3 551 Hijmans R J, van Etten J, M Sumner, J Cheng, D Baston, A Bevan, R Bivand *et al* 2020  
4 552 Geographic Data Analysis and Modeling, “raster”. R raster package, version 3.3-13. Available  
5 553 at: <https://r-spatial.org/raster>
- 6 554 Hugelius G, Strauss J, Zubrzych S, Harden J W, Schuur E A G, Ping C -L, Schirrmeister L, G  
7 555 Grosse, G J Michaelson, Koven C D, O'Donnell J A, Elberling B, Mishra U, Camill P, Yu Z,  
8 556 Palmtag J, and Kuhry P 2014 Estimated stocks of circumpolar permafrost carbon with  
9 557 quantified uncertainty ranges and identified data gaps *Biogeosciences* **11**. doi:10.5194/bg-11-  
10 558 6573-2014.
- 11 559 Jeong S-J, Bloom A A, Schimel D, Sweeney C, Parazoo N C, Medvigy D, Schaepman-Strub G,  
12 560 Zheng C, Schwalm C R, Huntzinger D N, Michalak A M, and Miller C E 2018 Accelerating  
13 561 rates of Arctic carbon cycling revealed by long-term atmospheric CO<sub>2</sub> measurements *Science*  
14 562 *Advances* **4** Doi: 10.1126/sciadv.ao1167.
- 15 563 Jones L A, Kimball J S, Reichle R H, N Madani, J Glassy, J V Ardizzone, A Colliander, J  
16 564 Cleverly, D Eamus, E Euskirchen, L Hutley, C Macfarlane, and R Scott 2017 The SMAP Level  
17 565 4 Carbon Product for Monitoring Ecosystem Land-Atmosphere CO<sub>2</sub> Exchange *IEEE*  
18 566 *Transactions on Geoscience and Remote Sensing* **55** 6517-6532.
- 19 567 Jorgenson M T, Harden J, Kanevskiy M, O'Donnell J, Wickland K, Ewing S, Manies K, Zhuang  
20 568 Q, Shur Y, Striegl R, and Koch J 2013 Reorganization of vegetation, hydrology and soil carbon  
21 569 after permafrost degradation across heterogeneous boreal landscapes *Environmental Research*  
22 570 *Letters* **8** 035017.
- 23 571 Jung M, Schwalm C, Migliavacca M, Walther S, Camps-Valls G, Koirala S, Anthoine P, Besnard  
24 572 S, Bodesheim P, Carvalhais N, Chevallier F, Gans F, Goll D S, Haverd V, Kohler P, Ichii K, Jain  
25 573 A K, *et al* 2020 Scaling carbon fluxes from eddy covariance sites to globe: synthesis and  
26 574 evaluation of the FLUXCOM approach *Biogeosciences* **17** 1343-1365.
- 27 575 Kasischke E S, Williams D, and Barry D 2002 Analysis of the patterns of large fires in the boreal  
28 576 forest region of Alaska *International Journal of Wildland Fire* **11** 131-144.
- 29 577 Kasischke E S, Hayes D J, Billings S, Boelman N, Colt S, Fisher J, Goetz S, Griffith P, Grosse  
30 578 G, Hall F, *et al* 2014 A concise experiment plan for the Arctic-Boreal Vulnerability Experiment.  
31 579 [cce.nasa.gov](http://cce.nasa.gov)
- 32 580 Kim Y, Ueyama M, Nakagawa F, Tsunogai U, Harazono Y, and Tanaka N 2006 Assessment of  
33 581 winter fluxes of CO<sub>2</sub> and CH<sub>4</sub> in boreal forest soils of central Alaska estimated by the profile  
34 582 method and chamber method: a diagnosis of methane emissions and implications for the regional  
35 583 carbon budget *Tellus B: Chemical and Physical Meteorology* **59** 223-233.
- 36 584 Kim Y, Kimball J S, Zhang K, and McDonald K C 2012 Satellite detection of increasing  
37 585 Northern Hemisphere non-frozen seasons from 1979 to 2008: implications for regional  
38 586 vegetation growth *Remote Sensing of Environment* **121** 472-487.
- 39 587 Kim Y, Kimball J S, Parazoo N, and Kirchner P 2021 Diagnosing environmental controls on  
40 588 vegetation greening and browning trends over Alaska and Northwest Canada using  
41 589 complementary satellite observations. In: Yang D, Kane D L (eds) *Arctic Hydrology, Permafrost*  
42 590 and Ecosystems. Springer, Cham. <https://doi.org/10.1007/978-3-030-50930-9-20>.

- 1  
2  
3 591 Kimball J S, Jones L A, Glassy J P, and Reichle R 2014 Soil Moisture Active Passive (SMAP)  
4 592 Algorithm Theoretical Basis Document SMAP Level 4 Carbon Data Product (L4\_C). Available  
5 593 at: [https://nsidc.org/sites/nsidc.org/files/files/271\\_L4\\_C\\_RevA\\_web.pdf](https://nsidc.org/sites/nsidc.org/files/files/271_L4_C_RevA_web.pdf)
- 6 594 Lasslop G, Reichstein M, Papale D, Richardson A D, Arneth A, Barr A, Stoy P, and Wohlfahrt G  
7 595 2010 Separation of net ecosystem exchange into assimilation and respiration using a light  
8 596 response curve approach: critical issues and global evaluation *Global Change Biology* **16** 187-  
9 597 208.
- 10 598 Li X and Xiao J 2019 Mapping photosynthesis solely from solar-induced chlorophyll  
11 599 fluorescence: A global, fine-resolution dataset of gross primary productivity derived from OCO-  
12 600 2 *Remote Sensing* **11** 2563. <https://doi.org/10.3390/rs11212563>.
- 13 601 Lin L C, Gerbig C, Wofsy S C, Andrews A E, Daube B C, Davis K J, and Grainger C A 2003 A  
14 602 near-field tool for simulating the upstream influence of atmospheric observations: The Stochastic  
15 603 Time-Inverted Lagrangian Transport (STILT) model *Journal of Geophysical Research  
Atmospheres* **108**. Available at: <https://doi.org/10.1029/2002JD003161>.
- 16 604 Liaw A and Wiener M 2002 Classification and regression by randomForest. *R News* **2** 18-22.  
17 605 ISSN 1609-3631.
- 18 606 Liaw A 2018 Classification and regression based on a forest of trees using random inputs, based  
19 607 on Breiman (2001). Version 4.6-14. Doi: 10.1023/A:1010933404324.
- 20 608 Liu Z, Kimball J S, Parazoo N C, Ballantyne A P, Wang W J, Madani N, Pan C G, Watts J D,  
21 609 Reichle R H, Sonnentag O, Marsh P, *et al* 2020 Increased high-latitude photosynthetic carbon  
22 610 gain offset by respiration carbon loss during an anomalous warm winter to spring transition  
23 611 *Global Change Biology* **26** 682-696.
- 24 612 Loboda T V, Hall A H, and Shevade V S 2017a ABoVE: Cumulative Annual Burned Area,  
25 613 Circumpolar High Northern Latitudes, 2001-2015. ORNL DAAC, Oak Ridge, Tennessee, USA.  
26 614 Available at: <https://doi.org/10.3334/ORNLDAA/1526>.
- 27 615 Loboda T V, Hall J V, and Baer A 2017b ABoVE: Wildlife date of burning within fire scars  
28 616 across Alaska and Canada, 2001-2019. ORNL DAAC, Oak Ridge, Tennessee, USA. Available  
29 617 at: <https://doi.org/10.3334/ORNLDAA/1559>.
- 30 618 Loboda T V, Hoy E E, and Carroll M L 2019 ABoVE: Study Domain and Standard reference  
31 619 grids, Version 2. Available at: <https://doi.org/10.3334/ORNLDAA/1527>.
- 32 620 Loranty M M, Berner L T, Taber E D, Kropp H, Natali S M, Alexander H D, Davydov S P,  
33 621 Zimov N S 2018 Understory vegetation mediates permafrost active layer dynamics and carbon  
34 622 dioxide fluxes in open-canopy larch forests of northeastern Siberia. *PLOS ONE*.  
35 623 <https://doi.org/10.1371/journal.pone.0194014>.
- 36 624 Luo D, Wu Q, Jin H, Marchenko S S, Lu L, and Gao S 2016 Recent changes in the active layer  
37 625 thickness across the northern hemisphere *Environmental Earth Sciences* **75** 55.  
38 626 <https://doi.org/10.1007/s12665-015-5229-2>.
- 39 627 Mahecha M D, Reichstein M, Carvalhais N, Lasslop G, Lange H, Seneviratne S I, *et al* 2010  
40 628 Global convergence in the temperature sensitivity of respiration at ecosystem level *Science* **329**  
41 629 838-840.
- 42 630 Meredith M, Sommerkorn M, Sassota S, Derksen C, Ekaykin A, Hollowed A, Kofinas G,  
43 631 Mackintosh A, Melbourne-Thomas J, Muelbert M M C, Ottersen G, Pritchard H, Schuur E A G,  
44 632

- 1  
2  
3 633 Boyd P, and Hobbs W 2019 Polar Regions. In: IPCC Special Report on the Ocean and  
4 634 Cryosphere in a Changing Climate [H-O Portner, D C Roberts, V Masson-Delmotte, et al (eds.)]  
5  
6 635 Minions C, Natali S, Watts J D, Ludwig S, and Risk D 2019 ABoVE: Year-round soil CO<sub>2</sub> efflux  
7 636 in Alaskan ecosystems, Version 2. ORNL DAAC, Oak Ridge, Tennessee, USA. Available at:  
8 637 <https://doi.org/10.3334/ORNLDAAAC/1762>.
- 9  
10 638 Myers-Smith I H, Kerby, J T, Phoenix G K, Bjerke J W, Epstein H E, Assmann J J, John C,  
11 639 Andreu-Hayles L, Angers-Blondin S, Beck P S A, Berner L T, Bhatt U S, Bjorkman A D, Blok  
12 640 D, Bryn A, Christiansen C T, Cornelissen J H C, Cunliffe A M, Elmendorf S C, Forbes B C, and  
13 641 Goetz S J, *et al* 2020 Complexity revealed in the greening of the Arctic *Nature Climate Change*  
14 642 **10** 106-117.
- 15  
16 643 Nagano H, Ikawa H, Nakai T, Matsushima-Yashima M, Kobayashi H, Kim Y, and Suzuki R  
17 644 2018 Extremely dry environment down-regulates nighttime respiration of a black spruce forest in  
18 645 Interior Alaska *Agricultural and Forest Meteorology* **249** 297-309.
- 19  
20 646 Natali S M, Schuur E A G, Webb E E, Hicks Pries C E, and Crummer K G 2014 Permafrost  
21 647 degradation stimulates carbon loss from experimentally warmed tundra *Ecology* **95** 602-608.
- 22  
23 648 Natali S M, Watts J D, Rogers B M, Potter S, Ludwig S M, Selbmann A-K, Sullivan P F, Abbott  
24 649 B W, Arndt K A, Birch L, Bjorkman M P, Bloom A A, Celis G, Christensen T R, Christiansen C  
25 650 T, Commane, R, Cooper E J, *et al* 2019 Large loss of CO<sub>2</sub> in winter observed across the northern  
26 651 permafrost region *Nature Climate Change* **9** 852-857.
- 27  
28 652 Oechel W C, Laskowski C A, Burba G, Gioli B, and Kalhori A A M 2014 Annual patterns and  
29 653 budgets of CO<sub>2</sub> flux in an Arctic tussock tundra ecosystem *Journal of Geophysical Research: Biogeosciences* **119** 323-339.
- 30  
31 654 O'Neill K P, Kasischke E S, and Richer D D 2002 Environmental controls on soil CO<sub>2</sub> flux  
32 655 following fire in black spruce, white spruce, and aspen stands of interior Alaska *Canadian Journal of Forest Research* **32** 1525-1541.
- 33  
34 656 O'Neill K P, Kasischke E S, and Richter D D 2003 Seasonal and decadal patterns of soil carbon  
35 657 uptake and emission along an age sequence of burned black spruce stands in interior Alaska  
36 *Journal of Geophysical Research: Atmospheres* **108** Doi: <https://doi.org/10.1029/2001JD000443>.
- 37  
38 660 Parmentier F J W, van der Molen M K, van Huissteden J, Karsanaev S A Kononov A V,  
39 661 Suzdalov D A, Maximov T C, and Doman A J 2011 Longer growing seasons do not increase net  
40 662 carbon uptake in the northeastern Siberian tundra *Journal of Geophysical Research: Biogeosciences* **116** G04013. Doi: 10.1029/2011JG001653.
- 41  
42 663 Parazoo N C, Commane R, Wofsy S C, Koven C D, Sweeney C, Lawrence D M, Lindaas J,  
43 664 Chang R Y-W, and Miller C E 2016 Detecting regional patterns of changing CO<sub>2</sub> flux in Alaska  
44 665 *PNAS* **113** 7733-7738.
- 45  
46 666 Parker T C, Clemmensen K E, Friggins N L, Hartley I P, Johnson D, Lindahl B D, Olofsson J,  
47 667 Siewert M B, Street L E, Subke J-A, and Wookey P A 2020 Rhizosphere allocation by canopy-  
48 668 forming species dominates soil CO<sub>2</sub> efflux in a subarctic landscape *New Phytologist* **227** 1818-  
49 669 1830.
- 50  
51 670 Pastick N J, Jorgenson M T, Goetz S J, Jones B M, Wylie B K, Minsley B J, Genet H, Knight J  
52 671 F, Swanson D K, and Jorgenson J C 2018 Spatiotemporal remote sensing of ecosystem change  
53 672 and causation across Alaska *Global Change Biology* **25** 1171-1189.
- 54  
55 673  
56 674  
57  
58  
59  
60

- 1  
2  
3 675 Pearson R G, Phillips S J, Loranty M M, Beck P S A, Damoulas T, Knight S J, and Goetz S J  
4 676 2013 Shifts in Arctic vegetation and associated feedbacks under climate change *Nature Climate  
5 Change* **3** 673-677.  
6  
7 678 Preskienis V, Laurion I, Bouchard F, Douglas P M J, Billett M F, Fortier D, and Xu X 2021  
8 679 Seasonal patterns in greenhouse gas emissions from lakes and ponds in a High Arctic polygonal  
9 680 landscape *Limnology and Oceanography* **66** S117-S141.  
10  
11 681 Pumpanen J, Kulmala L, Linden A, Kolari P, Nikinmaa E, and Hari P 2015 Seasonal dynamics  
12 682 of autotrophic respiration in boreal forest soil estimated by continuous chamber measurements  
13 683 *Boreal Environment Research* **20** 637-650.  
14  
15 684 Rawlins M A, McGuire A D, Kimball J S, Dass P, Lawrence D, Burke E, Chen X, Delire C,  
16 685 Koven C, MacDougall A, Peng S, and Rinke A, *et al* 2015 Assessment of model estimates of  
17 686 land-atmosphere CO<sub>2</sub> exchange across Northern Eurasia *Biogeosciences* **12** 4385-4405.  
18  
19 687 R Core Team 2019 R: a language and environment for statistical computing. R Foundation for  
20 688 Statistical Computing, Vienna, Austria. ISBN 3-900051-07-0, URL Available at: <http://www.R-project.org/>.  
21  
22 690 Reichstein M, Falge E, Baldocchi D, Papale D, Aubinet M, Berbigier P, Bernhofer C, Buchmann  
23 691 N, Gilmanov T, *et al* 2005 On the separation of net ecosystem exchange into assimilation and  
24 692 ecosystem respiration: review and improved algorithm *Global Change Biology* **11** 1424-1439.  
25  
26 693 Ribeiro-Kumara C, Koster E, Aaltonen H, and K Koster 2020 How do forest fires affect soil  
27 694 greenhouse gas emissions in upland boreal forests? A review. *Environmental Research* **184**  
28 695 109328. <https://doi.org/10.1016/j.envres.2020.109328>.  
29  
30 696 Rouse W R, Bello R L, D'Souza A, Griffis T J, and Lafleur P M 2002 The annual carbon budget  
31 697 for fen and forest in a wetland at Arctic treeline. *Arctic*, 55: 229-237.  
32  
33 698 Running S, Mu Q, and Zhao M 2015 MOD17A2H MODIS/Terra Gross Primary Productivity 8-  
34 699 Day L4 Global 500 SIN Grid V006. NASA EOSDIS Land Processes DAAC.  
35 700 <https://doi.org/10.5067/MODIS/MOD17A2H.006>.  
36  
37 701 Schiferl L D, Arndt A K, Biraud S C, Euskirchen E S, Henderson J M, Larson E J L, McKain K,  
38 702 Mountain M E, Munger J M, Oechel W C, Sweeney C, Watts J D, Yi Y, Zona D, and Commane  
39 703 R (In Review) Uncertainty in regional net CO<sub>2</sub> budget on the Alaskan North Slope driven by  
40 704 ability to constrain early winter CO<sub>2</sub> flux to the atmosphere. variable tundra ecosystem behavior  
41 705 and distribution. Submitted to *Proceedings of the National Academy of Sciences*.  
42  
43 706 Schimel D, Pavlick R, Fisher J B, Asner G P, Saatchi S, Townsend P, Miller C, Frankenberg C,  
44 707 Hibbard K, and Cox P 2015 Observing terrestrial ecosystems and the carbon cycle from space  
45 708 *Global Change Biology* **21** 1762-1776.  
46  
47 709 Schimel D, Schneider F D, *et al* (2019) Flux towers in the sky: global ecology from space *New  
48 710 Phytologist* **224** 570-584.  
49  
50 711 Schuur E A G, and Trumbore S E 2006 Partitioning sources of soil respiration in boreal black  
51 712 spruce forest using radiocarbon *Global Change Biology* **12** 165-176.  
52  
53 713 Schuur E A G, Vogel J G, Crummer K G, Lee H, Sickman J O, and Osterkamp T E 2009 The  
54 714 effect of permafrost thaw on old carbon release and net carbon exchange from tundra *Nature* **459**  
55 715 556-559.  
56  
57  
58  
59  
60

- 1  
2  
3 716 Schuur E A G, McGuire A D, Schadel C, Grosse G, Harden J W, Hayes D J, Hugelius G, Koven  
4 717 C D, Kuhry P, Lawrence D M, Natali S M, Olefeldt D, Romanovsky V E, Schaefer K, Turetsky  
5 718 M R, Treat C C, and Vonk J E 2015 Climate change and the permafrost carbon feedback *Nature*,  
6 719 **520** 171-179.  
7 720 Schuur E A G, and Mack M C 2018 Ecological response to permafrost thaw and consequences  
8 721 for local and global ecosystem services *Annual Review of Ecology, Evolution, and Systematics*,  
9 722 **49** 279-301.  
10 723 Sommerkorn M, Bolter M, and Kappen L 1999 Carbon dioxide fluxes of soils and mosses in wet  
11 724 tundra of Taimyr Peninsula, Siberia: controlling factors and contribution to net system fluxes  
12 725 *Polar Research* **18** 253-260.  
13 726 Stocks B J, Mason J A, Todd J B, Bosch E M, Wotton B M, Amiro B D, *et al* 2002 Large forest  
14 727 fires in Canada, 1959-1997 *Journal of Geophysical Research: Atmospheres* **108** 5-12.  
15 728 Street L E, Shaver G R, Williams M, and Van Wijk M T 2006 What is the relationship between  
16 729 changes in canopy leaf area and changes in photosynthetic CO<sub>2</sub> flux in arctic ecosystems?  
17 730 *Journal of Ecology* **95** 139-150.  
18 731 Strimbeck G R, Graae B J, Lang S, and Sorensen M V 2018 Functional group contributions to  
19 732 carbon fluxes in arctic-alpine ecosystems *Arctic, Antarctic, and Alpine Research* **51** 58-68.  
20 733 Tramontana G, Ichii K, Camps-Valls G, Tomelleri E, and Papale D 2015 Uncertainty analysis of  
21 734 gross primary production upscaling using Random Forests, remote sensing and eddy covariance  
22 735 data *Remote Sensing of Environment* **168** 360-373.  
23 736 Ueyama M, Iwata H, Nagano H, Tahara N, Iwama C, and Harazono Y 2019 Carbon dioxide  
24 737 balance in early-successional forests after forest fires in interior Alaska *Agricultural and Forest  
25 738 Meteorology* **275** 196-207.  
26 739 Wang T, Ciais P, Piao S L, Ottle C, Brender P, Maignan F, Arian A, Cescatti A, Gianelle D,  
27 740 Gouth C, Gu L, Lafleur P, Laurila T, Marcolla B, Margolis H, Montagnani L, *et al* 2011 Controls  
28 741 on winter ecosystem respiration in temperate and boreal ecosystems *Biogeosciences* **8** 2009-  
29 742 2025.  
30 743 Wang J A, Sulla-Menashe D, Woodcock C E, Sonnentag O, Keeling R F, and Friedl M A 2019  
31 744 ABoVE: Landsat-derived annual dominant land cover across ABoVE core domain, 1984-2014.  
32 745 ORNL-DAAC, Oak Ridge, Tennessee, USA. Available at:  
33 746 <https://doi.org/10.3334/ORNLDAA/1691>.  
34 747 Welker J M, Fahnstock J T, and Jones M H 2000 Annual CO<sub>2</sub> flux in dry and moist Arctic  
35 748 tundra: field responses to increases in summer temperatures and winter snow depth *Climatic  
36 749 Change* **44** 139-150.  
37 750 Wickland K P, Striegl R G, Neff J C, and Sachs T 2006 Effects of permafrost melting on CO<sub>2</sub>  
38 751 and CH<sub>4</sub> exchange of a poorly drained black spruce lowland *Journal of Geophysical Research  
39 752 Biogeosciences* **111** G02011 doi:10.1029/2005JG000099.  
40 753 Zona D, Gioli B, Commane R, Lindaas J, Wofsy S C, Miller C E, Dinardo S J, S Dengel,  
41 754 Sweeney C, Karion A, *et al* 2016 Cold season emissions dominate the Arctic tundra methane  
42 755 budget. *PNAS* **113** 40-45.  
43 756  
44 757  
45  
46  
47  
48  
49  
50  
51  
52  
53  
54  
55  
56  
57  
58  
59  
60